#### **ORIGINAL ARTICLE**



# Three-dimensional analysis of ductular reactions and their correlation with liver regeneration and fibrosis

Tadashi Yoshizawa<sup>1,2</sup> · Jae W. Lee<sup>1</sup> · Seung-Mo Hong<sup>1,3</sup> · DongJun Jung<sup>1,4</sup> · Michaël Noë<sup>5</sup> · Wojciech Zbijewski<sup>6</sup> · Ashley Kiemen<sup>7</sup> · Pei-Hsun Wu<sup>7</sup> · Denis Wirtz<sup>1,7</sup> · Ralph H. Hruban<sup>1,5</sup> · Laura D. Wood<sup>1,5</sup> · Kiyoko Oshima<sup>1</sup>

Received: 18 April 2023 / Revised: 24 August 2023 / Accepted: 30 August 2023 © The Author(s), under exclusive licence to Springer-Verlag GmbH Germany, part of Springer Nature 2023

#### **Abstract**

The liver has multiple regeneration modes, including hepatocellular hypertrophy and self-renewal of hepatocytes. When hepatocyte proliferation is impaired, hepatic progenitor cells may proliferate through ductular reaction (DR), differentiate into hepatocytes, and contribute to fibrosis. However, the three-dimensional spatial relationship between DR and regenerating hepatocytes and dynamic changes in DR associated with fibrosis remain poorly understood. Here, we performed three-dimensional (3D) imaging of cleared 42 liver explants with chronic and acute liver diseases and 4 normal livers to visualize DR. In chronic hepatic liver diseases, such as viral hepatitis, steatohepatitis, autoimmune hepatitis, and cryptogenic cirrhosis, the total length and number of branches of DR showed a significant positive correlation. We studied the spatial relationship between DR and GS-expressing cells using glutamine synthetase (GS) and cytokeratin 19 (CK19) as markers of liver regeneration and DR, respectively. The percentage of CK19-positive cells that co-expressed GS was less than 10% in chronic liver diseases. In contrast, nearly one-third of CK19-positive cells co-expressed GS in acute liver diseases, and chronic cholestatic liver diseases, including primary biliary cholangitis and primary sclerosing cholangitis, showed no co-expression. We also found that DR was longer and had more branching in livers with progressive fibrosis compared to those with regressive fibrosis. Our results suggest that DR displays varying degrees of spatial complexity and contribution to liver regeneration. DR may serve as hepatobiliary junctions that maintain continuity between hepatocytes and bile ducts rather than hepatocyte regeneration in chronic liver diseases.

Keywords Tissue clearing · Three-dimension · Ductular reaction · Liver · Liver regeneration · Glutamine synthetase

- Department of Pathology, Johns Hopkins University School of Medicine, Baltimore, MD, USA
- Department of Pathology and Bioscience, Hirosaki University Graduate School of Medicine, Hirosaki Aomori, Ianan
- Department of Pathology, Asan Medical Center, University of Ulsan College of Medicine, Seoul, Republic of Korea
- Department of Medicine, Graduate School, University of Ulsan, Seoul, Republic of Korea
- Department of Oncology, Johns Hopkins University School of Medicine, Baltimore, MD, USA
- Department of Biomedical Engineering, Johns Hopkins University, Baltimore, MD, USA
- Department of Chemical and Biomolecular Engineering, Johns Hopkins University, Baltimore, MD, USA

Published online: 14 September 2023

#### **Abbreviations**

| DR   | Ductular reaction    |
|------|----------------------|
| 3D   | Three-dimensional    |
| 2D   | Two-dimensional      |
| GS   | Glutamine synthetase |
| CK   | Cytokeratin          |
| DMSO | Dimethyl sulfoyide   |

DMSO Dimethyl sulfoxide
PBS Phosphate-buffered saline

DBE Dibenzyl ether

PSC Primary sclerosing cholangitis
PBC Primary biliary cholangitis

#### Introduction

Severe acute or chronic liver damage may lead to proliferation of hepatic progenitor cells (HPCs) that form pseudo ducts in a process termed ductular reaction (DR) [1, 2]. While DR is associated with hepatocyte regeneration and may lead to liver fibrosis



after regeneration, a role for DR in these processes remains controversial [3–5]. For example, although DR contributes to hepatocyte regeneration in zebra-fish [6, 7] and mouse model [8, 9] as well as in human diseases [2, 10–13], several studies that use cell lineage tracing analysis in mouse models have suggested that most hepatocytes regenerated after liver injury are derived from pre-existing hepatocytes [14, 15]. These conflicting results may stem from key differences that exist between animal models and human liver diseases, such as the duration of liver injury.

Previous studies on human liver tissues have primarily relied on two-dimensional (2D) or three-dimensional (3D) analysis based on the reconstruction of serial immunohistochemically labeled sections. However, physical sectioning of the tissue and reconstruction with alignment may artificially alter the structural relationship between key structures. Consequently, the precise 3D structure of DR and its spatial relationship with regenerating liver cells remain little understood. Recent advances in tissue clearing and imaging microscopy have enabled detailed 3D visualization of human tissues, including the pancreas and biliary tract, without sectioning [16–18]. These methods are superior to the reconstruction of serial immunohistochemically labeled sections because the continuity of bile ductules can be maintained and precisely visualized. Specifically, tissue clearing enables a reliable, quantitative assessment of the 3D structural relationship between bile ductules and hepatocytes. In our study, we determined the 3D architecture of DR and its spatial relationship with regenerating liver cells as well as dynamic changes in DR associated with fibrosis in human chronic and acute liver diseases using cleared liver tissues.

#### Materials and methods

#### **Patients and tissue collection**

After approval from the Johns Hopkins Institutional Review Board, 46 slabs  $(20 \times 1 \times 5 \text{ mm})$  of liver tissues

were obtained from patients who underwent liver transplantation or partial hepatectomy for the treatment of metastatic colonic adenocarcinoma at the Johns Hopkins Hospital (Table 1). To be consistent in tissue collection, all liver tissues were obtained from the hilar area. Normal liver tissues that were adjacent to metastatic adenocarcinoma were used as controls.

#### Fresh sample preparation

Fresh liver tissues were fixed for 24 h in 80% methanol and 20% dimethyl sulfoxide (DMSO). The tissues were then fixed in 4% paraformaldehyde for 24 h at 4 °C then immersed in 25% N,N,N',N'-tetrakis (2-hydroxypropyl) ethylenediamine solution (Millipore Sigma, St. Louis, MO, USA), 25% urea, 15% Triton X-100 (Millipore Sigma, St. Louis, MO, USA), and distilled water for 5 days at 37 °C to remove heme from hemoglobin [19]. Subsequently, tissues were washed three times with 1 x phosphate-buffered saline (PBS) for 1 h at 37 °C. After washing, tissues were dehydrated using methanol washes (one wash with 50%, 80%, and 90%, and two washes using 100% methanol). Tissues were then cooled for 1 h at 4 °C, incubated in 100% chloroform for 12 h at room temperature, and washed twice with 100% methanol. Subsequently, 5% hydrogen peroxide was added, and tissues were incubated overnight at 4 °C to oxidize endogenous pigments and autofluorescent proteins. Tissues were rehydrated through several washes  $(90\%, 80\%, \text{ and } 50\% \text{ methanol, followed by } 1 \times PBS)$  and washed twice for 1 h each in  $1 \times PBS/2\%$  Triton X-100. Finally, tissues were incubated for 2 days in a permeabilization solution of 1×PBS/20% DMSO/2% Triton X-100/0.3 mol/L glycine at 37 °C. Tissues were then incubated for 2 days in a blocking reagent consisting of 1×PBS/0.2% Triton X-100/10% DMSO/6% donkey serum.

**Table 1** Summary of liver samples

| Acute liver failure        |                                      | 2  |
|----------------------------|--------------------------------------|----|
| Chronic liver failure      |                                      | 40 |
| Hepatocyte damaged type    | cocyte damaged type                  |    |
|                            | Autoimmune Hepatitis                 | 5  |
|                            | Non-alcoholic Steatohepatitis        | 11 |
|                            | Alcoholic Hepatitis                  | 6  |
|                            | Hepatis C virus                      | 6  |
|                            | Hepatis B virus                      | 3  |
|                            | Cryptogenic Cirrhosis                | 2  |
| Cholangiocyte damaged type |                                      |    |
|                            | Primary Sclerosing Cholangitis (PSC) | 5  |
|                            | Primary Biliary Colangitis (PBC)     | 2  |
| Control                    |                                      | 4  |



**Table 2** Fibrosis staging of chronic hepatic liver diseases by Beijing classification

|  | Progressive | Intermediate | Regressive |
|--|-------------|--------------|------------|
| Autoimmune Hepatitis $(n=5)$           | 3           | 1            | 1          |
| Non-alcoholic Steatohepatitis $(n=11)$ | 11          |              |            |
| Alcoholic Hepatitis $(n=6)$            | 4           | 2            |            |
| Hepatis C virus $(n=6)$                | 4           | 1            | 1          |
| Hepatis B virus $(n=3)$                |             | 1            | 2          |
| Cryptogenic Cirrhosis $(n=2)$          | 2           |              |            |
| Total $(n=33)$                         | 24          | 5            | 4          |

# **Immunolabeling**

Whole-mount immunolabeling was performed as previously described [16–18] using two primary antibodies against CK19 (EP1580Y, rabbit monoclonal; final concentration, 1:200; Abcam, Cambridge, UK) and GS (mouse monoclonal, final concentration, 1:100, Abcam, Cambridge, UK). To enhance penetration of antibodies into liver tissues, the antibody concentration was gradually increased over 5 days. Centrifugal flow was also used to promote antibody penetration. During the 5-day antibody incubation perioid, tissues were repeatedly centrifuged for 12 h at  $500 \times g$  followed by shaking for 12 h at 37 °C. After primary antibody application, tissues were washed five times with  $1 \times PBS/0.2\%$  Tween-20 with 10-mg/mL heparin for 1 h each at room temperature and then incubated in Alexa Fluor 488-conjugated AffiniPure F(ab')2 fragment donkey anti-rabbit IgG (Jackson ImmunoResearch) and cyanine 3-conjugated AffiniPure F(ab')2 fragment donkey anti-mouse IgG (Jackson ImmunoResearch) for 4 days, protected from light. During this procedure, tissues were repeatedly centrifuged for 12 h at  $500 \times g$ , followed by shaking for 12 h at 37 °C. Tissues were then washed five times with  $1 \times PBS/0.2\%$  Tween-20 with 10-mg/mL heparin for 1 h each at room temperature.

### **Tissue clearing**

Tissues were dehydrated by several washes (once each with 50%, 80%, and 90% methanol, followed by three washes with 100% methanol) for 1 h each, followed by incubation with 66% dichloromethane/33% methanol for 3 h, and twice with 100% dichloromethane for 15 min. Finally, tissues were transferred to dibenzyl ether (DBE) overnight at 4 °C [20].

#### Tissue imaging

Cleared immunolabeled tissues were imaged using a Light Sheet Microscope (Ultramicroscope II; LaVision BioTec, Bielefeld, Germany) to obtain low-power views of larger tissue volumes. This microscope was equipped with a Neo sCMOS camera (Andor Technology, Belfast, UK) and a 4×objective lens immersed in DBE in the imaging chamber. A confocal laser scanning microscope (LSM800; Carl Zeiss, Jena, Germany) with 5×, 10×, and 20×objectives was used to obtain more detailed images of smaller tissue volumes using higher magnification lenses. Alexa 488 signals, indicating CK19 antibody labeling, were visualized using a bandpass filter set with an excitation range of 480/40 nm and an emission range of 421/50 nm. Cyanine 3 signals, indicating GS antibody labeling, were visualized using a filter set with excitation and emission ranges of 550/40 and 570/50 nm, respectively. Surface rendering image and 3D constructions were performed using IMARIS software (Ver. 9.4, Bitplane, Zurich, Switzerland).

#### Validation of cleared tissue observations

Tissues located adjacent to fresh liver tissues that were harvested for clearing were processed to create formalin-fixed paraffin-embedded (FFPE) blocks, which were cut into 4-µm thick sections and stained with hematoxylin and eosin (H&E) for microscopic examination. Masson's trichrome staining was used to assess liver fibrosis. H&E and Masson's trichrome staining of chronic liver tissues were evaluated by two pathologists (TY and KO) and classified into progressive, intermediate, or regressive stages of fibrosis according to the Beijing classification [21] (Fig. 1A–I, Table 2). Additionally, CK19 immunolabeling was performed on FFPE sections from the same patients to ensure that the DR captured on 3D images was comparable to DR represented on FFPE sections.

# Pathological evaluation and statistical analysis

Surface rendering and filament tracer analysis of IMARIS software were used to observe and analyze the 3D morphology of DR. Unit volume was determined by the diameter of cirrhotic nodule (R) and the formula R/2×R/4×R/8 (Suppl. Figure 1). The length and number of branching points of DR per unit volume were calculated through a filament tracer



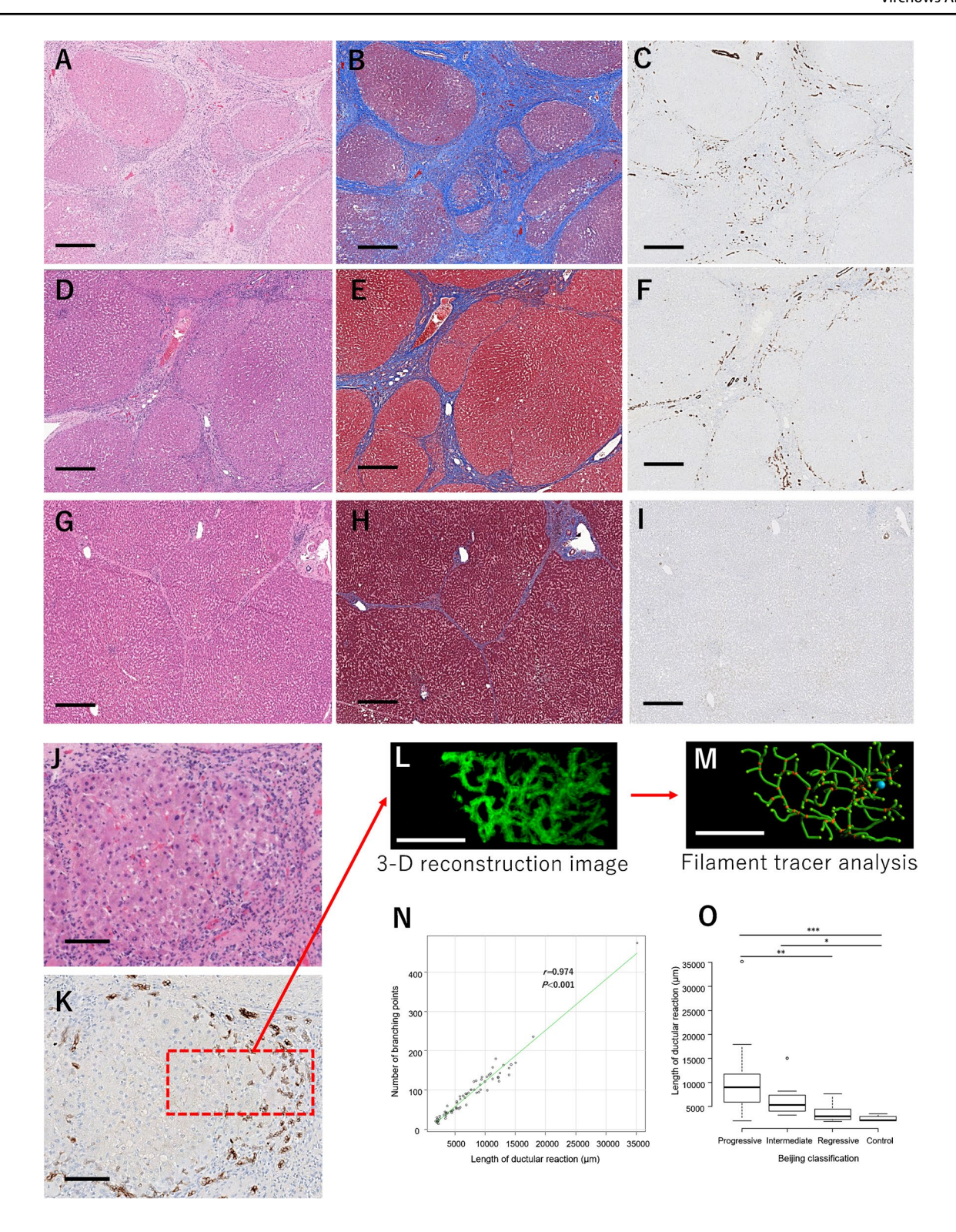
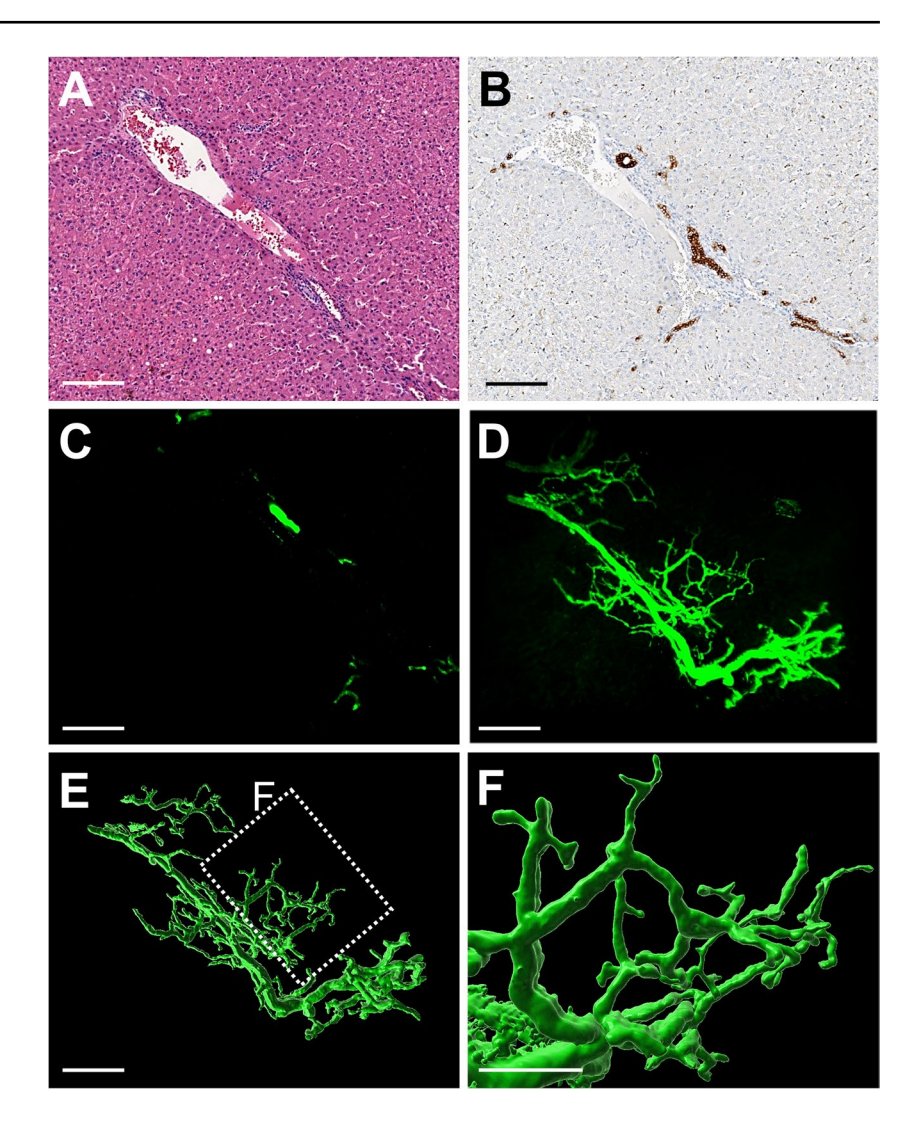


Fig. 1 Chronic hepatic liver diseases with progressive, intermediate, and regressive stages of fibrosis. A, B, C Images of chronic hepatic liver disease with progressive fibrosis, D, E, F intermediate fibrosis, G, H, I and regressive fibrosis. H&E stain (A, D, G), Masson's trichrome stain (B, E, H), and CK19 stain (C, F, I) are shown. Scale bar represents  $100 \ \mu m$ . J, K H&E and CK19 stains of chronic hepatic

liver with progressive fibrosis. Red square indicates the area analyzed for DR. L 3D surface rendering image of DR. M 3D filament tracer image of DR. N Correlation between the length of DR and the number of branches. O Quantification of the length of the DR. For control, the length of the normal bile ductules is shown. \*p < 0.05, \*\*p < 0.01, \*\*\*p < 0.001



Fig. 2 Structure of bile ducts in control liver. A H&E stain demonstrating the portal vein and interlobular bile ducts. B, C CK19 highlighting interlobular bile ducts in the portal triad. D 3D surface rendering image of bile ducts obtained from cleared liver tissue. E, F 3D surface rendering images of bile duct with branching. Scale bar represents 100 μm



analysis (Fig. 1J–M). Surface rendering analysis was performed to measure the GS-expressing cell volume, and the relationship between the cell volume and DR length was analyzed. The volumes of GS and CK19 co-expression regions per unit volume were also measured using the IMARIS colocalization software. Isolated bile ductules that expressed

GS in perivenular areas were not included in analysis. Variables were compared using Kruskal–Wallis multiple comparisons with Dunn's test. Spearman's rank correlation test was used to evaluate the association between DR and overall GS-expressing cell volume. R statistical programming language (http://r-project.org) was used for statistical analyses.

**Table 3** Co-expression rates of DR and GS

|         |                               | Co-expression cells (%) | Beijing Classification |
|---------|-------------------------------|-------------------------|------------------------|
| Case 1  | Autoimmune Hepatitis          | 1~5                     | Intermediate           |
| Case 2  | Non-alcoholic Steatohepatitis | 1~5                     | Progressive            |
| Case 3  | Non-alcoholic Steatohepatitis | 5~10                    | Progressive            |
| Case 4  | Non-alcoholic Steatohepatitis | 5~10                    | Progressive            |
| Case 5  | Non-alcoholic Steatohepatitis | <1                      | Progressive            |
| Case 6  | Non-alcoholic Steatohepatitis | 1~5                     | Progressive            |
| Case 7  | Non-alcoholic Steatohepatitis | 1~5                     | Progressive            |
| Case 8  | Alcoholic Hepatitis           | <1                      | Intermediate           |
| Case 9  | Hepatitis C virus             | <1                      | Intermediate           |
| Case 10 | Hepatitis B virus             | <1                      | Intermediate           |



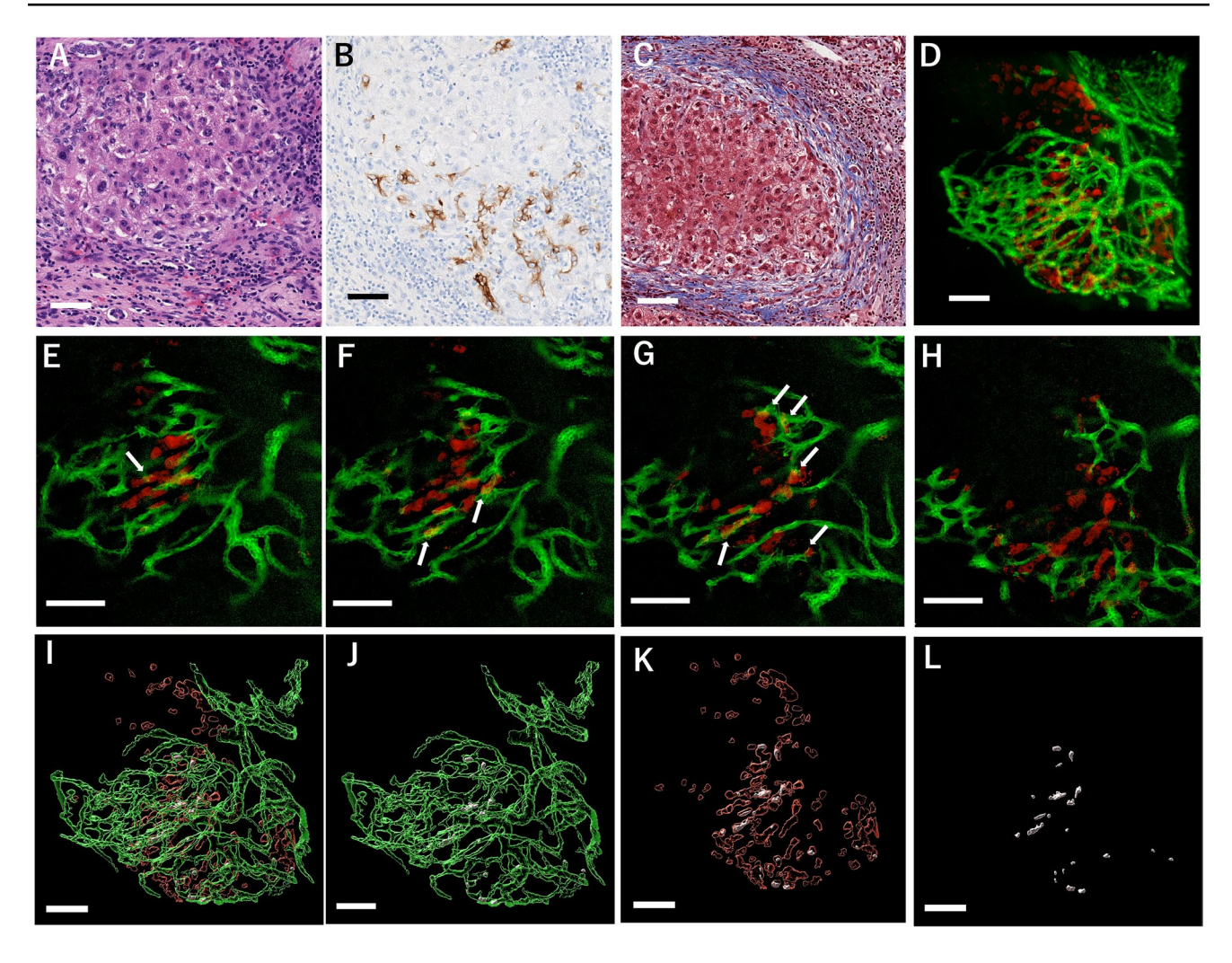


**Fig. 3** Chronic hepatic liver diseases. **A** H&E stain. **B** CK19 stain highlighting DR. **C** Masson's trichrome stain showing cirrhotic nodule. **D** 3D surface rendering image of DR and GS-positive cells (CK19, green; GS, red). **E–H** Serial 3D surface rendering images of DR and GS (images obtained every 9 μm). **I**, **J** 3D surface rendering

images of DR and GS-expressing cells. Areas of co-expression are shown in silver. K 3D surface rendering image of GS and co-expression area. L 3D surface rendering image of co-expression area only. Scale bar represents 100  $\mu m$ 

Results with p-values < 0.05 were considered statistically significant.

# Results

#### 3D analysis of normal intrahepatic bile ducts

To visualize the 3D structure of normal intrahepatic bile ducts, we examined liver tissues that were resected for the treatment of metastatic colon adenocarcinoma. Liver tissues that were not involved by metastatic disease showed normal liver histologic features with no evidence of fibrosis or inflammation on routine 2D microscopy (Fig. 2A), and CK19 highlighted interlobular bile ducts at the center of the portal triad and ductules at the periphery of the

portal triad. While 2D imaging did not reveal continuity of interlobular bile ducts to bile ductules (Fig. 2B, C), 3D imaging enabled visualization of branching of bile ducts (Fig. 2D). Surface rendering images showed that interlobular bile ducts became narrower and more branched toward the periphery to become bile ductules (Fig. 2E, F, Suppl. Movie 1). Together, 3D analysis enabled detailed visualization of the interconnected network of bile ductules with multiple branching points.

### 3D filament tracer analysis of DR

To examine whether the spatial complexity of DR is correlated with the staging of fibrosis, we used CK19 as a marker of DR and performed filament tracer analysis to determine



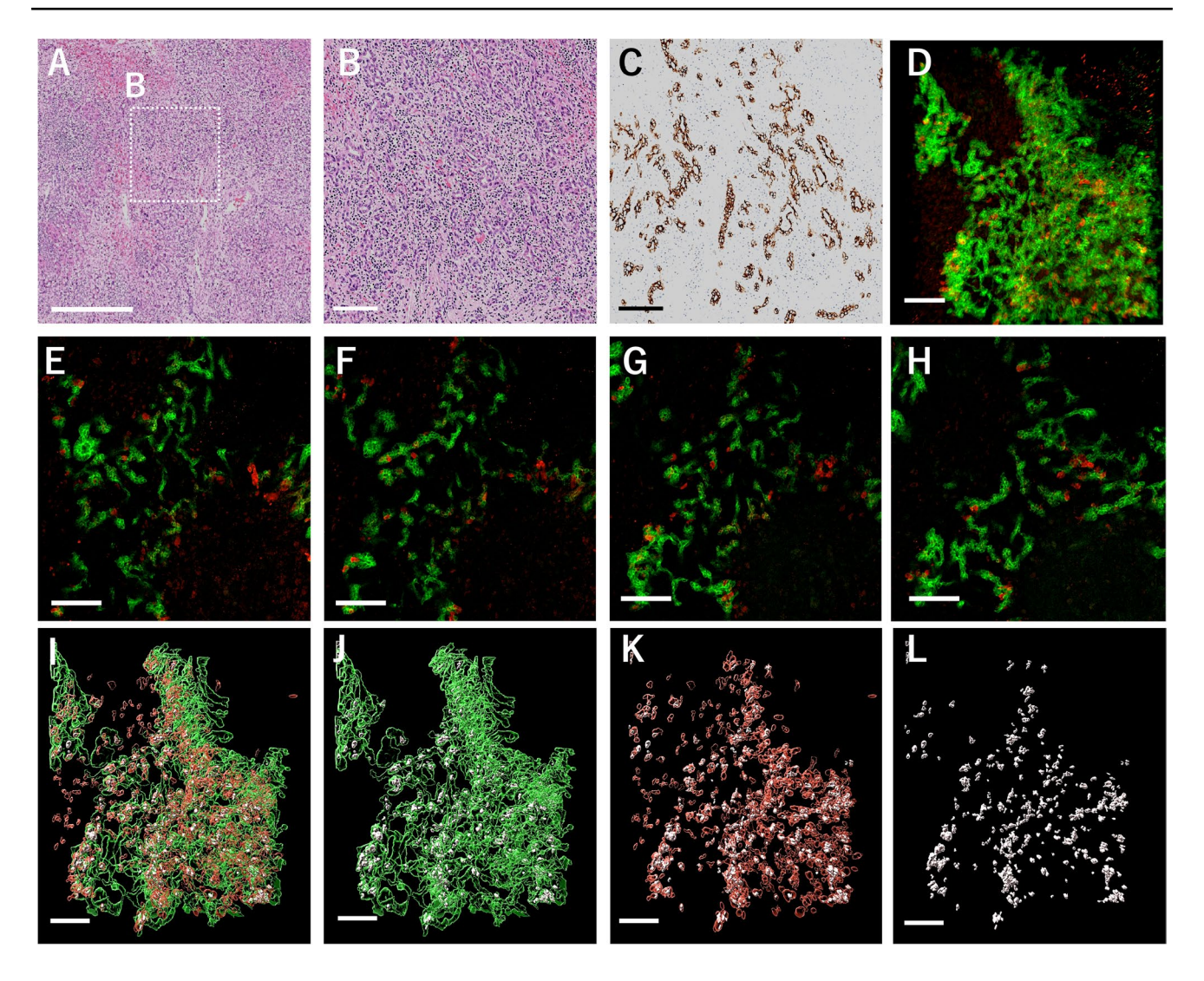


Fig. 4 Acute liver diseases. A, B H&E stain showing extensive hepatocytes necrosis associated with DR and severe inflammation. C CK19 stain highlighting exuberant DR. D 3D surface rendering image of DR and GS (CK19, green; GS, red). E–H Serial 3D surface rendering images of DR and GS (images obtained every 9  $\mu$ m). I, J 3D surface

rendering images of DR and GS-expressing cells. Areas of co-expression are shown in silver. **K** 3D surface rendering image of GS and co-expression area. **L** 3D surface rendering image of co-expression area only. Scale bar represents  $100 \, \mu m$ 

the length of DR and number of branches per unit volume in chronic hepatic liver diseases (Suppl. Figure 1). We found that these parameters were positively correlated (Fig. 1N), suggesting that longer DR is associated with increased spatial complexity. The length of DR was also compared among liver tissues with progressive, intermediate, and regressive stages of fibrosis as defined by the Beijing classification. DR was significantly longer in liver tissues with progressive and intermediate stages of fibrosis compared to the length of the normal bile ductules in the control group. Furthermore, DR was significantly longer in liver tissues with the progressive stage of fibrosis than the regressive stage of fibrosis (Fig. 1O).

# Co-expression of CK19 and GS in chronic hepatic liver diseases

To study the role of DR in liver regeneration, we evaluated liver tissues with chronic hepatic diseases for the co-expression of CK19 and GS, which were used as markers of DR and liver regeneration, respectively. Although DR was not readily identified by H&E or Masson's trichrome staining, CK19 immunolabeling highlighted DR in hepatic lobules with no visible tubular formation in 2D histologic sections (Fig. 3A-C). 3D imaging, on the other hand, revealed DR forming complex interconnected branches, and GS-positive cells, most of which were hepatocytes, were located near DR (Fig. 3D). Some cells that positive



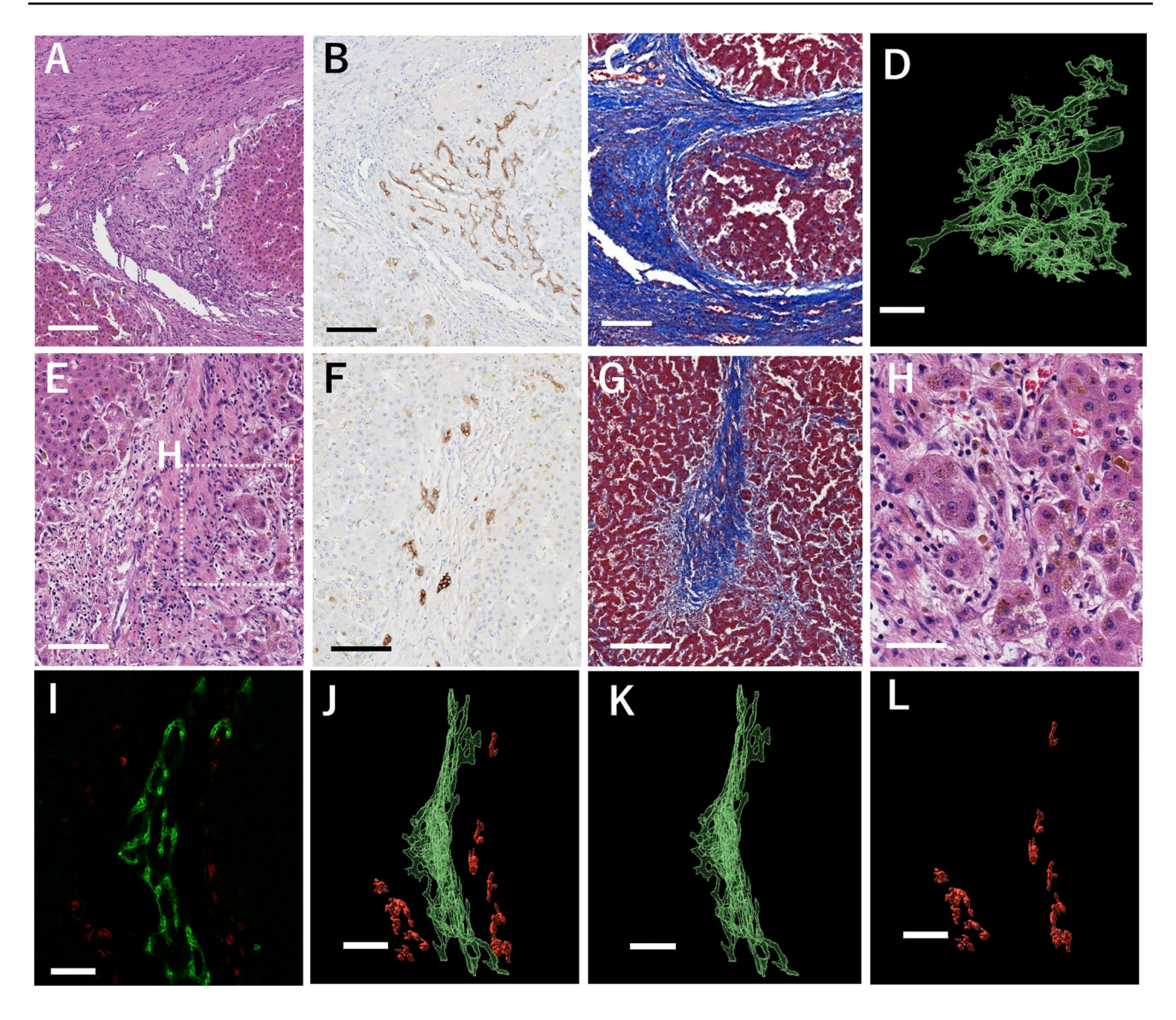


**Fig. 5** Chronic cholestatic liver diseases (primary sclerosing cholangitis). **A** H&E stain. **B** CK19 stain highlighting DR. **C** Masson's trichrome stain showing cirrhotic nodule with extensive fibrosis. **D** 3D surface rendering image of DR revealing continuously elongated DR. **E**, **F** H&E and CK19 stains showing DR. **G** Masson's trichrome stain

highlighting fibrosis. **H** Higher power of H&E stain showing DR and bile stasis in the surrounding hepatocytes and canalicular space. **I**, **J** 3D 3D surface rendering images of DR and GS-expressing cells. **K** 3D surface rendering image of DR. **L** 3D surface rendering image of GS-expressing cells. Scale bar represents  $100 \, \mu m$ 

for GS also co-expressed CK19 (Fig. 3E-L, Suppl. Movie 2). Among 17 GS-positive cases, cells co-expressing CK19 and GS were identified in 10 cases (58.8%) with 0.23–9.5% of CK19-positive cells co-expressing GS (Table 3). No apparent correlation was identified between the presence of CK19 and GS expression and underlying diseases.

# Co-expression of CK19 and GS in acute and chronic cholestatic liver diseases

In livers with acute diseases, hepatic parenchyma showed extensive necrotic associated severe inflammation (Fig. 4A, B) and robust DR, as highlighted by CK19 (Fig. 4C), in routine 2D histology. Visualization in 3D revealed that the branching of DR was more frequent compared to DR observed in chronic hepatic liver diseases (Fig. 4D). GS-positive cells were located near DR, and many CK19-positive cells (30.2–32.4%) co-expressed GS (Fig. 4E-L, Suppl. Movie 3). These results suggest that DR contributes more to liver regeneration in acute liver diseases compared to chronic hepatic liver diseases. In addition, we analyzed livers with chronic cholestatic diseases, including 5 cases of primary sclerosing cholangitis (PSC) and 2 cases of primary biliary cholangitis (PBC). GS-positive cells were



identified in 2 out of 5 PSC cases and 2 out of 2 PBC cases. Although GS-expressing cells were located close to DR, GS and CK19 co-expression was not observed (Fig. 5A–L). Together, these findings suggest that liver regeneration in chronic cholestatic liver diseases is less mediated by DR compared to chronic hepatic liver diseases.

#### Discussion

Mechanisms underlying hepatocyte regeneration are complex and remain poorly understood. Previous studies on hepatocyte regeneration revealed three key mechanisms: hepatocellular hypertrophy [22], self-renewal of hepatocytes [14, 15], and hepatocyte regeneration involving HPCs through a process called DR. Frequently associated with inflammation, DR refers to the histological expansion of epithelial cells that arise at the hepatocellular-biliary boundary in the setting of hepatocytes injury [2, 3, 6–12]. Studies have demonstrated that HPCs are present in the canals of Hering in acute and chronic liver failures that occur in the setting of acetaminophen-induced massive necrosis and cirrhosis, respectively [3, 11, 12]. There is a significant correlation between the number of HPCs and the extent of DR [4]. Notably, a prior 3D structure study on DR that relied on serial immunohistochemical stains showed that the canals of Hering contain HPCs [3]. In a more recent study, DR was shown to be critical for liver regeneration when hepatocytes undergo massive necrosis, whereas hepatocyte proliferation plays a larger role in mild liver injury [13]. However, the spatial relationship between DR and regenerating hepatocytes in different types and stages of liver injury remain little understood.

In our study, we utilized 3D imaging of cleared liver tissues to examine the role of DR in liver regeneration of multiple etiologies. First, we used 3D image analysis to calculate the percentage of CK19-positive cells that co-expressed GS to determine the frequency of DR in liver regeneration. GS is an enzyme normally expressed by hepatocytes surrounding the central veins. GS expression is associated with activation of the Wnt/β-catenin pathway [23, 24], and recent studies have shown that GS is a useful marker of liver regeneration and HPCs [12, 25, 26]. In chronic hepatic liver diseases, GS-expressing cells were located near DR and consisted predominantly of hepatocytes. Only a small percentage (0.23–9.5%) of CK19-expressing cells co-expressed GS. These findings are consistent with a recent study that utilized cell fate analysis in animal models to demonstrate that 0.78–2.45% of regenerating hepatocytes are derived from HPCs [27]. Our results are also consistent with a prior study that demonstrated only a modest role for DR in liver regeneration in the setting of chronic injuries [28],

in which DR may serve as hepatobiliary junctions that maintain continuity between hepatocytes and bile ducts rather than differentiating into hepatocytes.

In chronic cholestatic liver diseases, no cells co-expressed CK19 and GS, and GS was primarily expressed by hepatocytes. These findings suggest that DR does not play a significant role in liver regeneration in chronic cholestatic liver diseases. In contrast to chronic liver diseases, significantly higher levels of CK19 and GS co-expression (30.2–32.4%) were observed in acute liver diseases. In acute liver failure with massive hepatic necrosis, HPCs as well as  $\alpha$ -fetoprotein-positive acinar-arranged hepatocytes have previously been proposed to play a significant role in liver regeneration [12]. Our findings are supportive of the idea that DR has a major role in liver regeneration in the setting of acute liver diseases.

Furthermore, to understand the role of DR in different stages of fibrosis, we examined livers with chronic hepatic diseases and classified them according to the Beijing classification. Though liver fibrosis was once believed to be irreversible, advanced medical treatment has changed this concept. Increasing evidence shows that regression of fibrosis can occur in livers affected by chronic diseases, including viral hepatitis and autoimmune hepatitis [21, 29]. Our results show that livers with progressive fibrosis have longer DR with more branching than those with regressive fibrosis. These findings support recent studies that demonstrated a correlation between DR and fibrosis and a potential role for DR in progressive periportal fibrosis [4, 30]. In combination with prior studies, our results suggest that DR is a dynamic process that may evolve during the various stages of fibrosis.

Our study has a few limitations. First, liver tissues were obtained from patients with advanced liver diseases requiring transplantation. Therefore, changes that occur in the liver secondary to treatments and other factors, including infection and portal hypertension, may have influenced our results. In addition, our study did not evaluate the association between DR and liver regeneration in the early stage of chronic and acute liver diseases. Furthermore, our analysis of acute liver failure was limited to two cases, and additional studies are necessary to further validate our results. Second, we focused our study on DR, but cells other than hepatocytes and HPCs, including macrophages [31] and bone marrow cells [32], have been implicated in mediating liver regeneration. Third, we used small slabs of liver tissue measuring up to 20 mm for 3D studies. To ensure that these tissues were representative of the whole liver and to be consistent in our collection method, liver slabs were taken from only the hilar region of the explanted liver with diffuse disease involvement. We also performed H&E and Masson's trichrome stains on tissues that were adjacent to tissues harvested for clearing to ensure that histologic features observed on these stains were consistent with 3D findings.



Taken together, our study elucidated 3D structural processes underlying liver regeneration using tissue clearing technique. We reveal that DR contributes to liver regeneration and fibrosis in varying degrees and provide a detailed 3D understanding of the spatial relationship between DR and regenerating liver cells. Additional 3D-based studies on structural and molecular processes that orchestrate hepatocyte regeneration and fibrosis may enable identification of liver-intrinsic and extrinsic elements that can be targeted for therapeutic benefits.

**Supplementary Information** The online version contains supplementary material available at https://doi.org/10.1007/s00428-023-03641-3.

**Author contribution** TY and KO designed the study. TY, SH, and DJ performed experiments and data analysis. MN, WZ, AK, PW, and DW provided technical support. JWL, RHH, LDW, and KO performed data analysis and interpreted data. TY and KO developed methods and wrote the manuscript. All authors read and approved the manuscript.

**Funding** This study was supported by the Department of Pathology at the John Hopkins University School of Medicine.

**Data Availability** All data are available from the corresponding author upon reasonable requests.

#### **Declarations**

Studies were conducted in accordance with the 1996 Declaration of Helsinki and approved by the institutional review board (IRB) at the Johns Hopkins Hospital.

**Conflict of interest** The authors declare that they have no known competing financial interests or personal relationships that could have appeared to influence the work reported in this paper.

# References

- Roskams TA, Theise ND, Balabaud C, Bhagat G, Bhathal PS, Bioulac-Sage P et al (2004) Nomenclature of the finer branches of the biliary tree: canals, ductules, and ductular reactions in human livers. Hepatology 39:1739–1745. https://doi.org/10.1002/hep.20130
- 2. Popper H, Kent G, Stein R (1957) Ductular cell reaction in the liver in hepatic injury. J Mt Sinai Hosp NY 24:551–556
- 3. Theise ND, Saxena R, Portmann BC, Thung SN, Yee H, Chiriboga L et al (1999) The canals of hering and hepatic stem cells in humans. Hepatology 30:1425–1433. https://doi.org/10.1002/hep.510300614
- Richardson MM, Jonsson JR, Powell EE, Brunt EM, Neuschwander-Tetri BA, Bhathal PS et al (2007) Progressive fibrosis in nonalcoholic steatohepatitis: association with altered regeneration and a ductular reaction. Gastroenterology 133:80–90. https://doi.org/10.1053/j.gastro.2007.05.012
- Gouw AS, Clouston AD, Theise ND (2011) Ductular reactions in human liver: Diversity at the interface. Hepatology 54:1853– 1863. https://doi.org/10.1002/hep.24613
- Choi TY, Ninov N, Stainier DY, Shin D (2019) Extensive conversion of hepatic biliary epithelial cells to hepatocytes after near total loss of hepatocytes in zebrafish. Gastroenterology 146:776–788. https://doi.org/10.1053/j.gastro.2013.10.019
- 7. He J, Lu H, Zou Q, Luo L (2013) Regeneration of liver after extreme hepatocyte loss occurs mainly via biliary

- transdifferentiation in zebrafish. Gastroenterology 146:789-800. e8. https://doi.org/10.1053/j.gastro.2013.11.045
- Lu WY, Bird TG, Boulter L, Tsuchiya A, Cole AM, Hay T et al (2015) Hepatic progenitor cells of biliary origin with liver repopulation capacity. Nat Cell Biol 17:971–983. https://doi.org/10.1038/ncb3203
- Factor VM, Radaeva SA, Thorgeirsson SS (1994) Origin and fate of oval cells in dipin-induced hepatocarcinogenesis in the mouse. Am J Pathology 145:409–422
- Yoon SM, Gerasimidou D, Kuwahara R, Hytiroglou P, Yoo JE, Park YN et al (2011) Epithelial cell adhesion molecule (EpCAM) marks hepatocytes newly derived from stem/progenitor cells in humans. Hepatology 53:964–973. https://doi.org/10.1002/hep.24122
- Falkowski O, An HJ, Ianus IA, Chiriboga L, Yee H, West AB et al (2003) Regeneration of hepatocyte "buds" in cirrhosis from intrabiliary stem cells. J Hepatol 39:357–364. https://doi.org/10.1016/s0168-8278(03)00309-x
- 12. Stueck AE, Wanless IR (2015) Hepatocyte buds derived from progenitor cells repopulate regions of parenchymal extinction in human cirrhosis. Hepatology 61:1696–1707. https://doi.org/10.1002/hep.27706
- Dezső K, Nagy P, Paku S (2020) Human liver regeneration following massive hepatic necrosis: Two distinct patterns. J Gastroenterol Hepatol 35:124–134. https://doi.org/10.1111/jgh. 14721
- Yanger K, Knigin D, Zong Y, Maggs L, Gu G, Akiyama H et al (2014) Adult hepatocytes are generated by self-duplication rather than stem cell differentiation. Cell Stem Cell 15:340–349. https:// doi.org/10.1016/j.stem.2014.06.003
- Schaub JR, Malato Y, Gormond C, Willenbring H (2014) Evidence against a stem cell origin of new hepatocytes in a common mouse model of chronic liver injury. Cell Rep 8:933–939. https://doi.org/10.1016/j.celrep.2014.07.003
- Noë M, Rezaee N, Asrani K, Skaro M, Groot VP, Wu PH et al (2018) Immunolabeling of cleared human pancreata provides insights into three-dimensional pancreatic anatomy and pathology. Am J Pathol 188:1530–1535. https://doi.org/10.1016/j.ajpath. 2018.04.002
- Hong SM, Jung D, Kiemen A, Gaida MM, Yoshizawa T, Braxton AM et al (2020) Three-dimensional visualization of cleared human pancreas cancer reveals that sustained epithelial-to-mesenchymal transition is not required for venous invasion. Mod Pathol 33:639–647. https://doi.org/10.1038/s41379-019-0409-3
- Yoshizawa T, Hong SM, Jung D, Noë M, Kiemen A, Wu PH et al (2020) Three-dimensional analysis of extrahepatic cholangiocarcinoma and tumor budding. J Pathol 251:400–410. https://doi.org/ 10.1002/path.5474
- Tainaka K, Kubota SI, Suyama TQ, Susaki EA, Perrin D, Ukai-Tadenuma M et al (2014) Whole-body imaging with single-cell resolution by tissue decolorization. Cell 159:911–924. https://doi. org/10.1016/j.cell.2014.10.034
- Renier N, Wu Z, Simon DJ, Yang J, Ariel P, Tessier-Lavigne M et al (2014) iDISCO: a simple, rapid method to immunolabel large tissue samples for volume imaging. Cell 159:896–910. https://doi.org/10.1016/j.cell.2014.10.010
- Theise ND, Jia J, Sun Y, Wee A, You H (2018) Progression and regression of fibrosis in viral hepatitis in the treatment era: the Beijing classification. Mod Pathol 31:1191–1200. https://doi.org/ 10.1038/s41379-018-0048-0
- Miyaoka Y, Ebato K, Kato H, Arakawa S, Shimizu S, Miyajima A (2012) Hypertrophy and unconventional cell division of hepatocytes underlie liver regeneration. Curr Biol 22:1166–1175. https://doi.org/10.1016/j.cub.2012.05.016
- 23. Sekine S, Lan BY, Bedolli M, Feng S, Hebrok M (2006) Liverspecific loss of beta-catenin blocks glutamine synthesis pathway



- activity and cytochrome p450 expression in mice. Hepatology 43:817–825. https://doi.org/10.1002/hep.21131
- Cadoret A, Ovejero C, Terris B, Souil E, Lévy L, Lamers WH et al (2002) New targets of beta-catenin signaling in the liver are involved in the glutamine metabolism. Oncogene 21:8293–8301. https://doi.org/10.1038/si.onc.1206118
- Apte U, Singh S, Zeng G, Cieply B, Virji MA, Wu T et al (2010) Beta-Catenin Activation Promotes Liver Regeneration after Acetaminophen-Induced Injury. Am J Pathol 175:1056–1065. https://doi.org/10.2353/ajpath.2009.080976
- Fleming KE, Wanless IR (2013) Glutamine synthetase expression in activated hepatocyte progenitor cells and loss of hepatocellular expression in congestion and cirrhosis. Liver Int 33:525–534. https://doi.org/10.1111/liv.12099
- Español-Suñer R, Carpentier R, Van Hul N, Legry V, Achouri Y, Cordi S et al (2012) Liver progenitor cells yield functional hepatocytes in response to chronic liver injury in mice. Gastroenterology 143:1564-1575.e7. https://doi.org/10.1053/j.gastro.2012.08.024
- Clerbaux LA, Manco R, Van Hul N, Bouzin C, Sciarra A, Sempoux C et al (2019) Invasive ductular reaction operates hepatobiliary junctions upon hepatocellular injury in rodents and humans. Am J Pathology 189:1569–1581. https://doi.org/ 10.1016/j.ajpath.2019.04.011
- Wanless IR, Nakashima E, Sherman M (2000) Regression of human cirrhosis. Morphologic features and the genesis of

- incomplete septal cirrhosis. Arch Pathol Lab Med 124:1599–1607. https://doi.org/10.5858/2000-124-1599-ROHC
- Clouston AD, Powell EE, Walsh MJ, Richardson MM, Demetris AJ, Jonsson JR (2005) Fibrosis correlates with a ductular reaction in hepatitis C: roles of impaired replication, progenitor cells and steatosis. Hepatology 41:809–818. https://doi.org/10.1002/hep.20650
- Izumi T, Imai J, Yamamoto J, Kawana Y, Endo A, Sugawara H et al (2018) Vagus-macrophage-hepatocyte link promotes post-injury liver regeneration and whole-body survival through hepatic FoxM1 activation. Nat Commun 9:5300–5313. https://doi.org/10.1038/s41467-018-07747-0
- Petersen BE, Bowen WC, Patrene KD, Mars WM, Sullivan AK, Murase N et al (1999) Bone marrow as a potential source of hepatic oval cells. Science 284:1168–1170. https://doi.org/10. 1126/science.284.5417.1168

**Publisher's Note** Springer Nature remains neutral with regard to jurisdictional claims in published maps and institutional affiliations.

Springer Nature or its licensor (e.g. a society or other partner) holds exclusive rights to this article under a publishing agreement with the author(s) or other rightsholder(s); author self-archiving of the accepted manuscript version of this article is solely governed by the terms of such publishing agreement and applicable law.

